Nanomed J. 11(1): 80-92, Winter 2024

RESEARCH PAPER

Green synthesis of silver and cobalt oxide nanoparticles using *Croton macrostachyus* plant extract and evaluation of their antibacterial activity

Fikadu Worku Alemu [1], ***Tegene Desalegn Zeleke*** [1]*

[1]*Department of Applied Chemistry, Adama Science and Technology University, Ethiopia*

ABSTRACT

Objective(s): Cognizant of the harsh chemical method of nanoparticles synthesis, researchers are shifting towards the green phyto-mediated synthetic approaches. We herein report the green synthesis of Ag NPs and Co_3O_4 NPs using silver nitrate solution and cobalt nitrate solution as precursors added to aqueous extract of *Croton Macrostachyus* leaf extract to evaluate their antibacterial activity.

Materials and Methods: The Characterization of the biosynthesized NPs were carried out by using spectroscopic techniques as X-ray diffraction (XRD), UV-Vis spectroscopy, Fourier Transform Infrared (FTIR), and scanning electron microscopy (SEM).

Results: The average crystallite size of Ag NPs was found to be 12.62 nm from the XRD data, indicating a cubic crystal structure whereas that of Co_3O_4 NPs was found to be 12.75 nm, indicating a cubic spinel crystal structure. The energy band gap for Ag NPs and Co_3O_4 NPs were 3.38 eV, and 3.34 eV respectively. The SEM images showed non-homogeneity of particles distribution with irregular geometries attributable to their shape and size for Ag NPs whereas spherical as well as irregular geometries attributed to non-homogeneity of the particles for Co_3O_4 NPs. The FTIR identifies the functional groups of the bioactive molecules that were actively involved as stabilizing and capping agents to prevent agglomeration of Ag NPs and Co_3O_4 NPs. The agar-well diffusion method was employed to evaluate the antibacterial activities of the produced nanoparticles against gram-positive (*S. aureus* and *E. faecalis*) and gram-negative (*E. coli*, *S. typhimrium*) bacterial strains.

Conclusion: The biosynthesized nanoparticles showed promising antibacterial activities with Ag NPs exhibiting the best inhibition activities towards all bacteria species.

Keywords: *Antimicrobial resistance, Bacteria, Biosynthesis, Nanoparticles, Phytochemicals*

How to cite this article

Alemu FW, Zeleke TD. Green synthesis of silver and cobalt oxide nanoparticles using Croton macrostachyus plant extract and evaluation of their antibacterial activity. Nanomed J. 2024; 11(1): 80-92. DOI: 10.22038/NMJ.2023.75230.1826

INTRODUCTION

Antimicrobial resistance (AMR), has become a serious concern over the past years to the efficient management of an expanding array of infectious diseases brought on by bacteria, parasites, viruses, and fungi. Antibacterial, antiparasitic, antiviral, and antifungal medications become less effective as a result of AMR, making patient treatment challenging, expensive, or even unfeasible. The impact on particularly vulnerable patients is most obvious, resulting in prolonged illness and increased mortality [1]. The spread of multidrug-resistant bacteria, which cause frequent diseases and are difficult to treat with currently available antimicrobial drugs, is becoming more and more evident [2]. The common antibacterial agents that are currently being utilized exhibit various mechanisms such as cell wall synthesis, translational machinery, and DNA replication machinery. Inappropriately, bacterial resistance can develop against each of these modes of action. Therefore, the development of new drugs has become highly demanding. A plausible concept of drug improvement through effect enhancement using nanoparticles has become a potential alternative which allows the binding of metals, proteins, phospholipids, and antibodies [3].

The broad spectrum of antibacterial performance associated with high specific surface area of nanomaterials makes them the most

* *Corresponding author: Email: tegened@yahoo.com*

Note. This manuscript was submitted on September 28, 2023; approved on November 21, 2023

promising antimicrobial substances, and hence bacteria can hardly develop resistance pertaining to the complex antibacterial mechanism of nanomaterials. The majority of antibiotic resistance mechanisms are irrelevant for nanoparticles as their method of action involves direct interaction with the bacterial cell wall without the need to penetrate the cell. This increases the likelihood that NPs won't promote bacterial resistance more than antibiotics would. As a result, interest in novel and intriguing NP-based compounds with antibacterial activity has increased [4, 5].

Nanoparticles can be defined as at least one of their dimensions must fall below 100 nm.

However, the most intriguing characteristics of nanoparticles become apparent at sizes smaller than 10 nm. The surface-to-volume ratios of nanoparticles with dimensions are high. A nanoparticle can be zero dimensional, as in the case of nanodots, where its length, breadth, and height are all fixed at a single point; one dimensional, as in the case of graphene, where it can have only one parameter; two dimensional, as in the case of carbon nanotubes; or three dimensional, as in the case of gold nanoparticles, which have all three dimensions. The nanoparticles differ in size, structure, and form. Its size varies from 1 nm to 100 nm and can be spherical, cylindrical, tubular, conical, hollow core, spiral, flat, etc. Surface variations can result in an uneven or homogeneous surface. Amorphous or crystalline single- or multi-crystal solids that are either loose or clumped together can be found in some nanoparticles [6].

Several chemical, physical, and biological approaches are currently employed for the fabrication of nanoparticles. Conventional synthesis processes, encompassing both chemical and physical methods, are typically executed in severe environments. Unfortunately, the synthesis of nanoparticles using strong reducing agents and toxic organic solvents has put the environment at serious risk. Therefore, it is imperative to develop relatively cheap and environmentally friendly nanomaterials. In contrast, biological processes are typically carried out in ambient temperature and pressure, indicating simplicity, energy efficiency, and decreased toxicity or harm to the environment and human health. Utilization of microorganisms, enzymes, and plant extracts, in biological-based synthesis is thought to be the most environmentally benign substitute for physical and chemical techniques. Plant-based synthesis techniques are advantageous over other biological processes because they do away with the laborious process of maintaining cell cultures. Accordingly, the green synthesis is a better alternative to conventional synthesis as they are non-toxic, pollutant free and eco-friendly, economical and more sustainable. Plants contain a considerable number of both capping and reducing agents, such as flavonoids, polyphenols, and other reducing components, which can reduce salts to zero-valent and avoid agglomeration [7].

Owing to their unique qualities, nanoparticles are used extensively in a variety of sectors, including environmental remediation, electronics, biology and biomedical material science, cosmetics, physics, renewable energies, and catalysis. [8]. Silver nanoparticles (Ag NPs) have unique qualities that make them a viable choice for a range of applications. These properties include being an excellent catalyst, antibacterial agent, and biosensor. They can also be easily reduced from silver salts to generate zero-valent silver [9]. The distinctive and important applications of Co_3O_4 NPs have also attracted a lot of attention [10]. Co_3O_4 is a multipurpose antiferromagnetic p-type semiconductor that finds use in gas sensors, solar selective absorbers, energy storage, pigments and dyes, field emission materials, capacitors, heterogeneous catalysis, magneto-resistive devices, and electronic thin films. Furthermore, it finds usage in biological applications (drug transport, therapeutic agents, anti-cancer, antiviral, antifungal, antileishmanial, and antibacterial properties) [11-13]. Literature reports indicated that green synthesis methods have been used to prepare both silver and cobalt oxide nanoparticles for various applications [14, -18].

However, no reports were published related to the synthesis of Ag NPs and Co_3O_4 NPs by *C. macrostachyus* plant extract through the green chemistry approach. Therefore, the present work presents the phyto-mediated synthesis of silver NPs and cobalt NPs using *C. Macrostaychus* plant extract and evaluation of their antibacterial activity.

C. macrostachyus is one of the most abundant plant species in several African nations, such as Eritrea, Ethiopia, Kenya, Tanzania, and Uganda. It is a member of the *Euphorbiaceae* family's genus Croton L., which is also known as Croton within the subfamily *Crotonoideae.* This family includes about 1200 species of trees, shrubs, herbs, and

occasionally lianas. The genus Croton is used in traditionally for the treatment of multiple human health problems including diabetes, malaria, dysentery, stomachache, and ascariasis in different areas. Many bioactive substances have been found in *C. macrostachyus* fruits, leaves, stem bark, and twigs. These include alkaloids, amino acids, anthraquinones, carbohydrates, cardiac glycosides, coumarins, essential oil, fatty acids, flavonoids, phenolic compounds, phlobatannins, polyphenols, phytosteroides, saponins, sterols, tannins, terpenoids, unsaturated sterol, and vitamin C. [19-21]. Phytochemical screening of the aqueous extract of *C. macrostachyus* plant extract indicated the presence of tannins, anthocyanins saponin, phenolic compound, steroids, triterpens, alkaloids, coumarins, antraquinones, glucosides and essential oils [22]. These components play great role in the formation of metallic nanoparticles. They can also function as capping and reducing agents and are harmless for the environment and biodegradable. Water can be utilized as a more environmentally friendly solvent than organic solvents like hexane and ethanol, which is the primary advantage of aqueous extractions.

MATERIALS AND METHOD

Chemicals and reagents

In this study, Distilled water, cobalt(II) nitrate hexahydrate ($Co(NO_3)_2.6H_2O$), silver nitrate ($AgNO_3$), ethanol, sodium hydroxide (NaOH), Muller Hinton agar, H_2SO_4, $FeCl_3$, and *C. macrostachyus* plant were the ingredients and reagents needed to prepare Ag NPs and Co_3O_4 NPs. Every chemical that was employed was of the analytical grade. The *C. macrostachyus* plant was taken from its native habitat areas in Adea Berga,Woreda, Oromia Regional State The chemicals and reagents were purchased from chemical stores in Addis Ababa.

Instruments

The following laboratory tools were used to characterize the synthesized NPs: The optical characteristics of the nanoparticles were investigated using UV-Vis spectroscopy; the atoms' vibrational motions in the molecules of the synthesized Ag NPs and Co_3O_4 NPs were clarified using FITR; the nature of the nanoparticles' crystal structure was ascertained using XRD; and the morphology of the synthesized nanoparticles was depicted using SEM.

Preparation of the C. macrostachyus Plant Extract

The *C.macrostachyus* plant leaves were collected from its natural habitat areas of Oromia Regional State, West Showa, Adea Berga Woreda. Sample collection and preparation of *C. macrostachyus* leaf extract were carried out according to the literature of [22] with slight modifications. *C. macrostachyus* leaves were collected and washed thoroughly with deionized water to remove any dirt particles. The cleaned leaves were ground and allowed to air dry. A 1000 mL conical flask was filled with 18 g of powdered *C. macrostachyus* plant leaves. 600 mL of distilled water was then added, and the mixture was heated for 30 min at 70 °C. The heater was turned off after 30 min, and the mixture was agitated for an hour. The mixture was given some time to settle. Wattman No. 1 filter paper was used to filter the settled extract. It was kept in the refrigerator at 4 °C. Then, the prepared extract was used for the synthesis of Ag NPs and Co_3O_4 NPs.

Fig. 1 shows the schematic procedure for the preparation of the plant extract.

Phytochemical Qualitative Analysis of Aqueous Extract C. macrostachyus plant

In this study, the following established standard procedures were used to evaluate the plant leaf

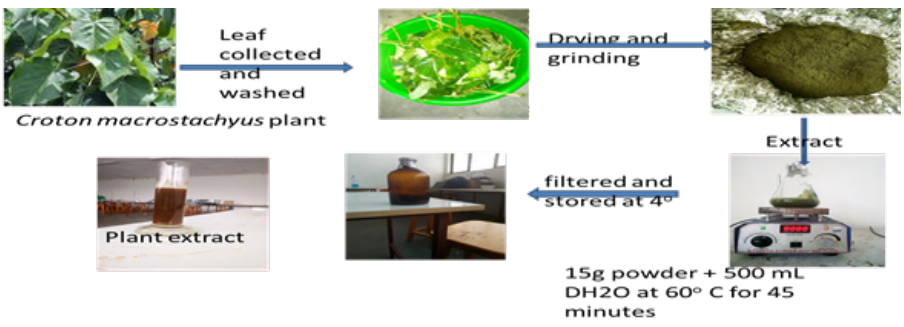

Fig. 1. Preparation of *Croton macrostachyus* plant extract

extract for the presence of phytochemicals [23].

Tests for flavonoids (Alkaline reagent test)

An aqueous plant crude extract was mixed with 2 mL of 2.0% NaOH; this resulted in a bright yellow tint that vanished when two drops of diluted acid were applied. This depicts the existence of flavonoids.

Test for tannins

(Ferric chloride test): A test tube containing 2 mL of plant leaf extract was heated to boiling. Five drops of 0.1% $FeCl_3$ were added to produce a blue-black or brownish-green tint, indicating the presence of tannins.

Test for terpenoids (Salkowski test)

A layer was formed by mixing 2 mL of aqueous plant extract with 2 mL of chloroform and 3 mL concentrated H_2SO_4 carefully to form a layer. Positive results for the presence of terpenoids were shown by the interface's reddish-brown coloring.

Test for steroids

2 mL of chloroform and 2 drops of concentrated H_2SO_4 were added to 5 mL aqueous solution of the plant crude extract. The appearance of the red color in the lower chloroform layer indicated the presence of steroids.

Tests for glycosides (Salkowski's test)

In this test, an aqueous plant extract was mixed with 2 mL of concentrated H_2SO_4. A reddish-brown hue developed, signifying the presence of the glycosides' steroidal aglycone component.

Test for phytosterols (Salkowski's test)

Following the addition of 10 mL of chloroform and 2 mL of aqueous plant extract, the mixture was filtered. After adding five drops of concentrated H_2SO_4 to the filtrate, the mixture was agitated to check if a golden yellow hue had appeared as the confirmation for the presence of phytosterols.

Test for saponins

The plant leaf extract (0.5 g) was taken and 5 mL of distilled water was added and shaken while heating to boil. The frothing observed showed the presence of saponins.

Test for phenols

5 drops of 2 % of $FeCl_3$ was added to 2 mL of aqueous solution of the plant leaf extract, and the resulting bluish-green color indicated the presence of phenols.

Procedure for synthesis of silver nanoparticles

The plant mediated synthesis of silver nanoparticles using *C. macrostachyus* leaf extract was carried out using the reported procedure [24] with minor modification. In this regard, an aqueous solution (0.2 M) of $AgNO_3$(aq) solution was made by dissolving 16.99 g of $AgNO_3$ salt in distilled water and shaking the content to prepare a homogeneous mixture. Finally, the distilled water was filled into the volumetric flask until its mark in a 500 mL volumetric flask. The Ag NPs were prepared by mixing 200 mL of 0.2 M silver nitrate solution with 200 mL of *C. macrostachyus* plant extract under stirring at 30 °C for 3 hr. The mixture was settled at room temperature for 24 hr and then, the solution was centrifuged for 20 min at 2000 rpm. The recovered solid portion was then washed in distilled water and ethanol before being dried for 24 hr on a ceramic crucible at 70°C in an Oven. Finally, the obtained dark brown colored powder was stored for further analysis.

Fig. 2. Synthesis of silver nanoparticle

Fig. 2 shows the schematic procedure for the preparation of silver nanoparticles.

Procedure for synthesis of Co_3O_4 nanoparticles

The phyto-mediated synthesis of Co_3O_4 nanoparticles in which *C. macrostachyus* leaf extract was used as capping agent has been carried out according to the literature report by [25] with minor modification. Here, an aqueous solution of (0.2 M) $Co(NO_3)2.6H_2O$(aq) solution was prepared by taking 29.1g of $Co(NO_3)2.6H_2O$) salt and added into 500 mL of volumetric flask followed by addition of distilled water. Then, the contents were shaken to get a homogenous mixture. The Co_3O_4NPs were prepared by mixing 200 mL of 0.2M $Co(NO_3)2.6H_2O$ solution with 200 mL of *C. macrostachyus* leaf extract under stirring at 60 °C for 5 hr. The mixture was settled at room temperature for 24 hr and then centrifuged for 20 min at 2000 rpm. Then, the obtained solid part was washed with distilled water and ethanol then dried on a ceramic crucible for 24 hr at 70 °C in Oven. Finally, the light-brown colored powder obtained was calcinated at 400 °C for 4 hr and the product was kept for further analysis.

Fig. 3 shows the schematic procedure for the preparation of Co_3O_4 nanoparticle.

Characterization of Ag NPs and Co_3O_4 NPs

The UV-Vis absorption peaks of the nanoparticles were measured using UV-Vis spectroscopy (V-770 UV-Visible/NIR spectrophotometer) in the 200–800 nm range. Spectra from an FTIR (FTIR-6600 FT-IR) spectrometer were obtained between 400 and 4000 cm^{-1}. The crystalline nature of the synthesized Ag NPs and Co_3O_4 NPs were studied with the aid of XRD. The powder sample was fully mixed with potassium bromide (KBr) and compressed using a hydraulic press to produce pellets before being put in the instrument's sample container. Then XRD instrument uses Cu-Kα radiation (λ=0.154056 nm) runs at 40 kV with an applied current of 30 mA and scans at a speed of 3.00 degrees per min. The data collected were scanned between the range of 2θ = 10° < 2θ ≤ 80°. The JEOL and JCM-6000Plus SEM was utilized to comprehend the morphological and structural characteristics of the produced NPs. NPs powder was put on a sample holder for SEM characterization, and then a conductive metal coating was applied. A finely focused electron beam was then utilized to scan the materials.

Procedure for antibacterial activity test

The synthesized Ag NPs and Co_3O_4 NPs were tested for *in vitro* antibacterial activities against four bacteria strains (*E .coli (*gram-negative), *S. aureus* (gram-positive), *E. faecalis* (gram positive), and *S. typhimirim* (gram negative)) by Agar disc diffusion method [26] at Adama public health referrals and research laboratory center. The bacterial stock cultures were maintained on the sheep blood agar slants at 37 °C. Freshly, grown liquid culture of the test strains having similar turbidity with 0.5McFarland were seeded over the Mueller-Hinton agar medium with sterile swab. The disc measuring 6 mm in diameter was prepared from Whatman filter paper sterilized by dry heat at 121 °C for 20 min. The different concentrations of Ag NPs and Co_3O_4 NPs (20, 10, 5 and, 2.5 mg/mL) were prepared by dissolving synthesized nanoparticles in DMSO. Then, sterilized 6 mm filter paper discs were soaked in each prepared

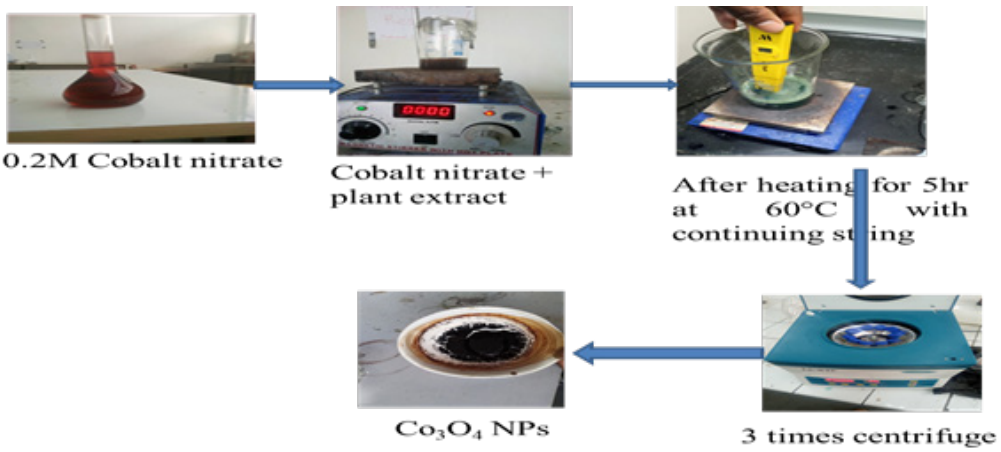

Fig. 3. syntheses of Co_3O_4 NPs

nanoparticles. The discs impregnated with the test solutions were placed on a cultured glass plate at an equal distance to one another to avoid overlap of zones of growth inhibitions.

The growth inhibition zone was measured in mm after 24 hr incubation at 37 °C and compared with the standard drug (Contrimoxazole). DMSO was used as a negative control and 25 µg Contrimoxazole was used as a standard drug (positive control). All the above procedure were repeated three times and mean standard deviation of a zone of inhibition were taken.

RESULTS AND DISCUSSION

The phytochemical screening test results

The first step in the phyto-mediated synthesis of the Ag NPs and Co_3O_4 nanoparticles was to prepare the aqueous extract of the *C. macrostachyus* plant from the dried and crushed plant leaf part. The isolated *C. macrostachyus* plant leaf extract was subjected to phytochemical screening in order to identify the phytochemicals involved in the capping and/or reduction of the nanoparticles during their synthesis. The summary of the phytochemical analysis results for the *C. macrostachyus* plant extract are presented in Table 1 and Fig. 4.

The analysis data obtained showed that the main constituents of the *C. macrostachyus* plant extract were flavonoids, tannins, terpenoids, glycosides, phytosterols, saponins, and phenols. These constituents are accountable for promoting the production of Ag NPs and Co_3O_4 NPs. Plant extracts' phytochemical constituents have stabilizing and reducing properties [27]. Literature reports verify that flavonoids can be employed as reducing agents in the process of creating biocompatible nanoparticles [28]. According to Ahmad et al. (2010), free hydrogen generated when flavonoids like luteolin and rosmarinic acid undergo ketoenol conversion can reduce Ag+ ions and make silver nanoparticles [29]. In a separate study, it has been demonstrated that the –OH group of flavonoids, such as myricetin and quercetin, can oxidize to carbonyl groups during the bioreduction of metal ions [30]. Polyphenols and terpenoids are used as both bioreducing and stabilizing agents. Plant extracts rich with saponins, tannins, glycosides, and phytosterol can support the synthesis of small-size nanoparticles [31, 32].

Table 1. Results of Phytochemical Screening of *Croton macrostachyus* plant extract

s.no	Secondary metabolite	Results
1	Flavonoid	+
2	Tannins	+
3	Terpenoid	+
4	Steroid	+
5	Phytosterols	+
6	Glycosides	+
7	Sapponins	+
8	Phenols	+

X-ray diffraction (XRD) analysis

The composition and crystal structure Ag NPs and Co_3O_4 NPs produced were ascertained by X-ray diffraction (XRD) analysis. The prepared samples' XRD results are displayed in Fig. 5. By comparing the experimentally acquired patterns to the typical Ag NPs and Co_3O_4 NPs patterns, analysis of the result has been made. Diffraction peaks for Ag NPs were observed at 2θ values of 38.15°, 44.23°, 64.48°, and 77.39°, respectively. These values correspond to the (111), (200), (220), and (311) planes, as shown in Fig. 5(a). The synthesized Ag NPs were found to be in cubic phase based on the

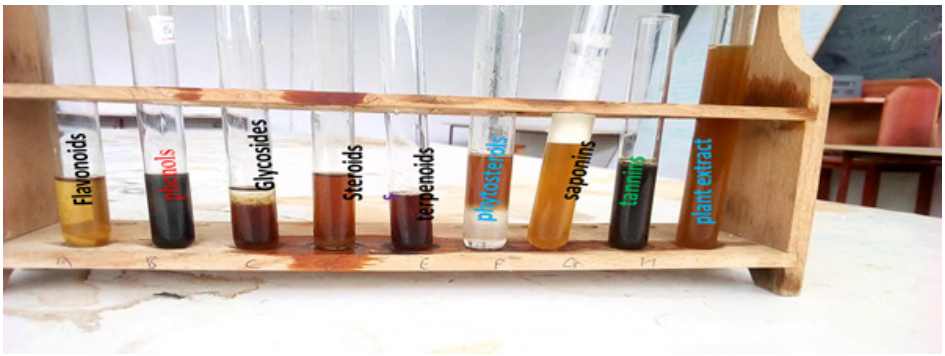

Fig. 4. Results of Phytochemical Screening of *Croton macrostachyus* plant extract

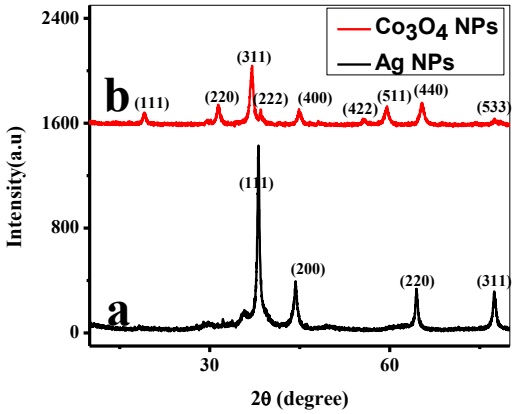

Fig. 5. X-ray diffraction patterns a) Ag NPs and b) Co_3O_4 NPs

spectral data, and the detected peaks were fitted using space group Fm-3m of the Joint Committee on Powder Diffraction Standard (JCPDS card No. 004-0783).

The XRD pattern of Co_3O_4 NPs is shown in Fig. 5(b). The diffractogram shows that the diffraction peaks were observed at 2θ = 19.19°, 31.47, 37.07°, 38.73°, 44.96°, 55.73°, 59.47°, 65.34°, and 77.42°, respectively. These values correspond to the Miller indices (hkl) values of (111), (220), (311), (222), (400), (422), (511), (440), and (533). A cubic spinel crystal structure was proposed from recorded spectral data of the synthesized Co_3O_4 with the observed peaks perfectly fitted with the Joint Committee on Powder Diffraction Standard (JCPDS card No. 042-1467, space group Fd-3m).

The average crystallite size of the Ag NPs and Co_3O_4 NPs nanoparticles was estimated by using Scherrer‟s formula [33] equation (1).

$$D = \frac{K\lambda}{\beta \cos\theta} \quad (1)$$

Where D represents the average crystallite size, is average particle size, θ is the Bragg diffraction angle, λ refers to the X-ray wavelength (CuKα radiation and equals 0.15406 nm), and β is the FWHM of the XRD peak appearing at the diffraction angle θ.

For synthetic NPs, the dislocation densities are computed using;

$$\delta = \frac{1}{D^2} \quad (2)$$

Where D is the crystalline size and δ is the dislocation density, The micro-strain is estimated from;

$$\varepsilon = \frac{\beta}{4tan\theta} \quad (3)$$

The d-spacing (d), particle size (D), dislocation density (δ), microstrain (ε), of the Ag NPs and Co_3O_4 were computed. and presented in Table 2 and Table 3 for the strongest peaks of respective synthesized Ag NPs and Co_3O_4 NPs respectively.

There exists a correlation between the dislocation density (δ), microstrain (ε), average crystalline size (D), and peak position (2θ) that emanates from the entire set of derived data in

Table 2. The calculated parameters for the strongest peaks of Ag NPs

2θ	θ	β	D (nm)	D average (nm)	d-spacing	δ x 10^3 (nm^{-2})	ε x 10^{-3}
38.14	19.07	0.66	12.75	12.62	2.36	6.15	8.32
44.2	22.1	1.25	6.84		2.05	21.37	13.47
64.5	32.25	0.58	16.04		1.44	3.88	4.05
77.4	38.7	0.686	14.84		1.23	4.54	3.74

Table 3. The calculated parameters for the strongest peaks of Co3O4 NPs

2θ	θ	β	D(nm)	D average (nm)	d-spacing	δ x 10^3 (nm^{-2})	ε x 10^{-3}
19.19	9.6	0.645	12.49	12.75	4.62	6.41	16.65
31.47	15.74	0.64	12.87		2.84	6.04	9.93
37.00	18.50	0.66	12.70		2.43	6.2	8.6
38.73	19.37	0.76	11.08		2.32	8.14	9.43
44.96	22.48	0.7134	12.05		2.015	6.88	7.52
55.74	27.87	0.66	13.62		1.65	5.4	5.45
59.45	29.72	0.82	11.19		1.55	7.99	6.25
65.34	32.67	0.78	12.02		1.43	6.92	5.34
77.42	38.7121	0.61	16.69		1.23	3.59	3.32

the manner shown below: Peak position or angle (2θ) increased, as indicated by the decrease in microstrain (ε). Additionally, the average crystalline size grew as peak position increased, suggesting that crystalline size also contributed to peak broadening. Dislocation density is a measure of the number of dislocations in a unit volume of crystalline materials. Consequently, nanoparticle size increases with the decrease in the dislocation density of crystalline materials. Stated differently, the crystalline particle's dislocation density decreases with increasing peak position (angle).

The peak position (2θ) was increased in the Ag NPs and Co_3O_4 NPs, with average crystalline sizes of 12.62 nm and 12.75 nm, respectively. Dislocation density decreases with increasing particle size since it is dependent on particle size. Thus, the dislocation density of Co_3O_4 was greater than that of Ag NPs.

UV- Vis spectroscopy analysis

The optical properties in terms of absorption spectra and band gap energy of the synthesized Ag NPs and Co_3O_4 NPs are presented in Fig. 6 and Fig. 7 respectively. The Ag NPs showed absorption bands at 402 nm as shown in Fig. 6 (a). The result confirms the formation of silver nanoparticles by exhibiting the typical surface plasmon resonance absorption characteristic of the Ag NPs. The coupled vibrating of free electrons in resonance with light waves is what gives metal nanoparticles their surface plasmon resonance characteristic features [34]. Equation (4) describes the relationship between a direct band gap semiconductor's absorption coefficient and band gap energy, Eg, in the parabolic band structure.

$$(\alpha hv)2 = A(hv - Eg) \quad (4)$$

In this case, v is the frequency of the photon, A is the slope in the linear region, and_ is the Planck's constant. Equation (5) was obtained by using the remission function in Equation (2) and taking the K–M scattering coefficient S as a constant with respect to wavelength.

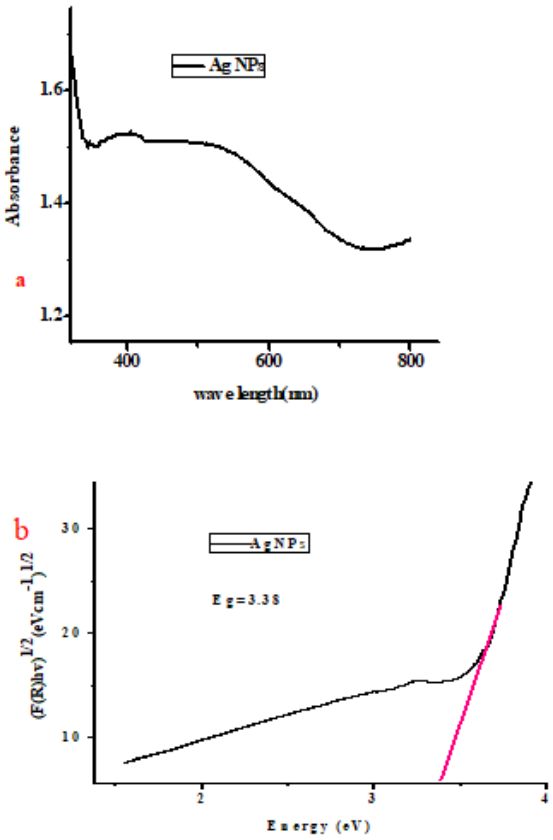

Fig. 6. (a) Wavelength versus Absorbance of UV-Vis spectroscopy, (b) energy versus band gap of Ag NPs

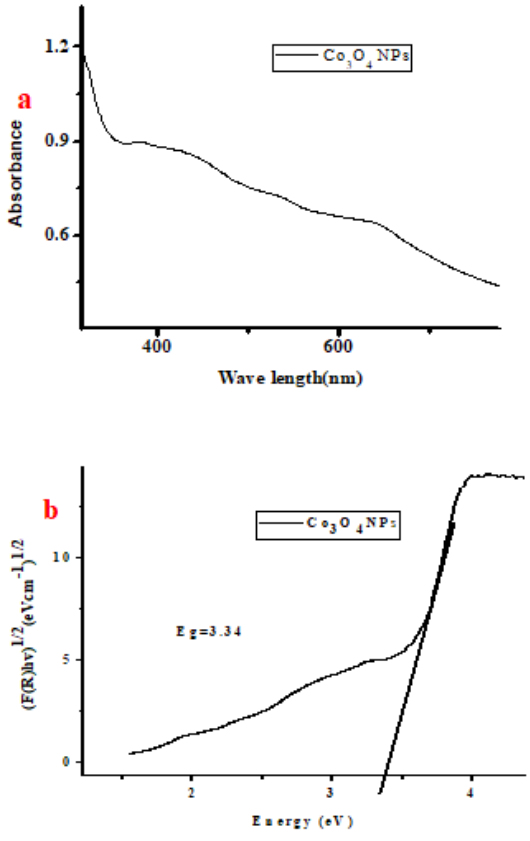

Fig. 7. (a) Wavelength versus Absorbance of UV-Vis spectroscopy, (b) energy versus band gap of Co_3O_4 NPs

$$(F(R)\mathrm{h}v)2 = A(\mathrm{h}v - Eg) \quad (5)$$

Where, F(R) is equal to K/S, the molar absorption coefficient K is equal to (1 – R)2, the scattering factor S is equal to 2R, and R is the reflectance of the materials and is defined as %R/100. The linear part of Kubelka–Munk (K–M) plots was extrapolated to calculate the direct and indirect bandgap energies of the nanomaterials [35].

The plots are displayed in Fig. 6(b), which shows that the band gap of the silver nanoparticles is 3.38 eV. The bandgap energy for the nanoparticles was calculated using the Tauc relations, which are presented in equation (5).

Whenever photon energy with the maximum absorbance wavelength (λmax) is received, the intra-band gap excitation of conduction electrons from the lowest energy state to higher energy levels around the Fermi level of the conduction band determines the absorption band of light in metal nanoparticles. A smaller particle size may have less of an attraction between its metal ions and conduction electrons since it contains fewer atoms. As a result, the particle's conduction band energy rises. However, because larger particles have more atoms, there is a greater potential for attraction between conduction electrons and metal ions, which lowers the conduction band energy of the metal nanoparticles [36].

The cobalt ion remains in two distinct oxidation states (Co^{3+} and Co^{2+}), which could account for the two absorption peaks seen in the UV-Vis spectroscopy. The formation of absorption bands was caused by the charge transfer processes from O^{2-} to Co^{2+} and O^{2-} to Co^{3+}, which results in larger band gap and lower band gap energies, respectively. The two absorption peaks observed between 500-580 nm and 600-680 nm respectively for Co_3O_4 nanoparticles, were in good agreement with the previous reports [37]. According to Eltarahony et al., the first band can be linked to the process of $O^{2-} \rightarrow Co^{2+}$ charge transfer, while the second band is linked to $O^{2-} \rightarrow Co^{3+}$ charge transfer, indicating the possibility of cobalt oxide synthesis. Surface plasmon absorption peak (SPR) at 400–450 nm was discovered, as shown in Fig. 7(a). The SPR phenomenon is caused by metallic nanoparticles physically absorbing light, which causes the metal's conduction electrons to oscillate coherently [38].

As seen in Fig. 7(b), the energy band gap of Co_3O_4 NPs was determined to be 3.34 eV as a result of the electron forming holes in the valence band adjacent to the conduction band. Because of the quantum confinement effect, the optical band gap energy raises the potential well of small lateral dimensions of cobalt oxide nanoparticles. Due to its two distinct oxidation states, the cobalt ion functions as a p-type semiconductor. The transfer of O^{2-} between the filled and unoccupied oxygen sides is caused by the positive hole exchange between Co^{3+} and Co^{2+}. Thus, the Co_3O_4 system exhibits d-d charge transfer and p-type semiconducting material [39].

Scanning electron microscopy (SEM) analysis

Fig. 8(a) and 8(b) demonstrate the morphology and texture of the synthesized Ag NPs and Co_3O_4NPs as shown by SEM micrographs. The SEM image of the synthesized Ag NPs is shown in Fig. 8 (a). The shape and size of the particles were not uniform, as demonstrated by the micrograph.

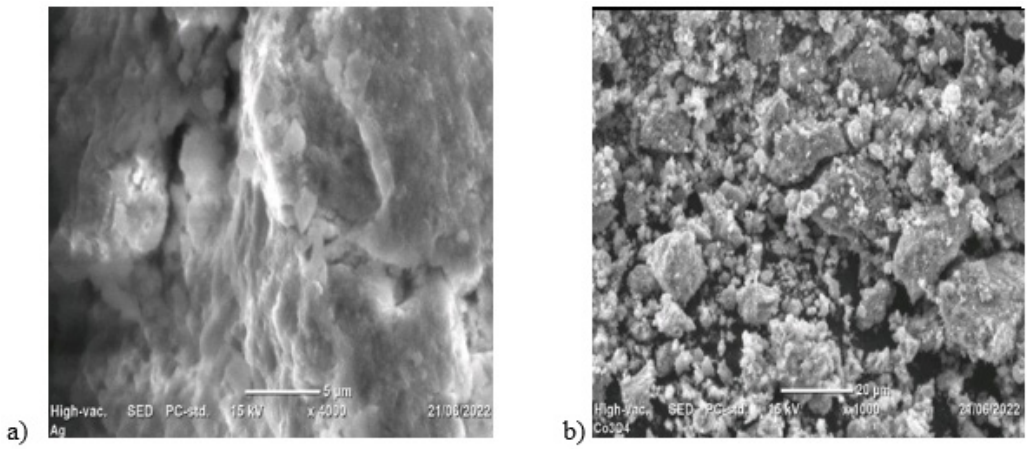

Fig. 8. SEM image of (a) Ag NPs (b) Co3O4 NPs

Different particle sizes and irregular geometries of Ag NPs were observed. The SEM scans of Co_3O_4 NPs in Fig. 8(b) showed the nonhomogeneous nature of the particles in terms of size and shape. The micrographs illustrate the spherical and irregular geometries of the Co_3O_4 NPs, as well as the range of particle sizes detected in the micrographs.

Fourier transform infrared (FT-IR) spectroscopy analysis

To investigate the synthesis of Ag NPs and Co_3O_4 NPs, as well as to validate the functional groups present in the leaf extract of the *C. macrostachyus* plant leaf extract, FTIR analysis was performed on the green synthesized nanoparticles, and the leaf extract of the *C. macrostachyus* plant. This is used to pinpoint the bioactive compounds that actively participated in the production process as capping and stabilizing agents to stop Ag NPs and Co_3O_4 NPs from growing further. The FT-IR results of the Croton macrostachyus plant leaf extract, Ag NPs, and Co_3O_4 NPs are displayed in Fig. 9.

The FTIR spectrum of *C. macrostachyus* plant leaf extract presented in Figure 9(a) showed the absorption bands at 3432 cm^{-1}, 2920 cm^{-1}, 2114 cm^{-1}, 1641 cm^{-1}, 1444 cm^{-1}, 1020 cm^{-1} and 543 cm^{-1}. The existence of O-H stretching is confirmed by the large peak in the spectra seen at about 3432 cm^{-1}. Whereas, the absorption peak observed at about 2920 cm^{-1} confirmed the presence of the alkane's C-H stretching vibrations. Nitrile (C ≡ N) functional groups are represented by the peak that was seen at about 2114 cm^{-1}. A peak at 1641 cm^{-1} showed the presence of amide (C=O) stretch and the peak at 1444 cm^{-1} refers to N-H bend of primary amines and bending of C-H alkanes. The absorptions peak

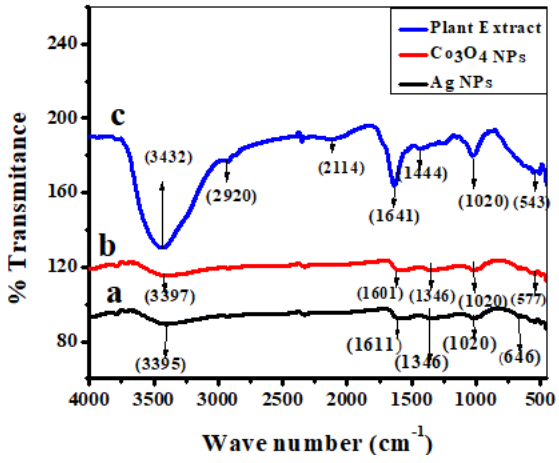

Fig. 9. FTIR spectra of (a) Ag NPs, b) Co_3O_4 NPs, (c) plant extract

at around 1020 cm^{-1} C-O stretch was attributed to the ether functional group. The peak at 543 cm^{-1} correspond to the presence of aryl disulfide (S–S) or Polysulfides (S–S stretch) or C–Br stretch.

The FTIR spectra of the synthesized Ag NPs and Co_3O_4 NPs shown in Figure 9(b and c) clearly indicated that some peak shifting expressed in terms of change in peak strength, increase, or disappearance were observed.

The shifts in peaks indicated that the binding of the functional groups with the nanoparticles involved. After the synthesis process, the peaks at 3432 cm^{-1}, 2920 cm^{-1}, 2114 cm^{-1}, 1641 cm^{-1}, 1444 cm^{-1}, 1020 cm^{-1} and 543 shifted to 3395 cm^{-1}, 1611 cm^{-1}, 1346 cm^{-1} and 1020 cm^{-1} and 646 cm^{-1} for Ag NPs. The absorption band at 3395 cm^{-1} corresponds to –OH stretching of the carboxylic acid. While, the peak at 1611 cm^{-1}, 1346 cm^{-1} indicates N=O Stretch of the Nitro Groups and N=O Bend of the nitro group. The absorption peak at 1020 cm^{-1} indicated C-O stretch of the ether functional group and the absorption peak at 646 cm^{-1} may be due to Ag-O bond [40-42].

For Co_3O_4 NPs, the absorption peaks observed at 3397 cm^{-1}, 1601, 1346 cm^{-1}, 10420 cm^{-1} and 646 cm^{-1} as shown on Fig. 9 (c) also confirmed the involvement of organic moieties in the binding process. The absorption peak at 3397 cm^{-1} corresponds to –OH stretching of the carboxylic acid. The peaks observed at 1601 cm^{-1} may be due to C=C stretching. 1346 cm^{-1} and 1020 cm^{-1} corresponds to N=O Bend of the nitro group and C-O stretch of the ether functional group respectively. The absorption peak observed at 577 cm^{-1} corresponds to the stretch Co-O present in cobalt oxide nanoparticles [43-45]. Hydroxyl-rich phenolics like phenolic acids and flavonoids are act as reducing agents for metal ions and Most of the studies reported the same molecule used as both reducing and capping agents [46, 47].

Antibacterial activity of synthesized Ag NPs and Co_3O_4 NPs

This section presents antibacterial properties of the synthesized NPs. The antibacterial activity of the green produced Ag NPs and Co_3O_4NPs was investigated using the agar disc diffusion assay technique. As seen in Fig. 10 and 11, the Ag NPs and Co_3O_4 NPs had antibacterial action against gram-positive (*S. aureus* and *E. faecalis*) and gram-negative (*E. coli* and *S. typhimirium*) bacterial strains, respectively.

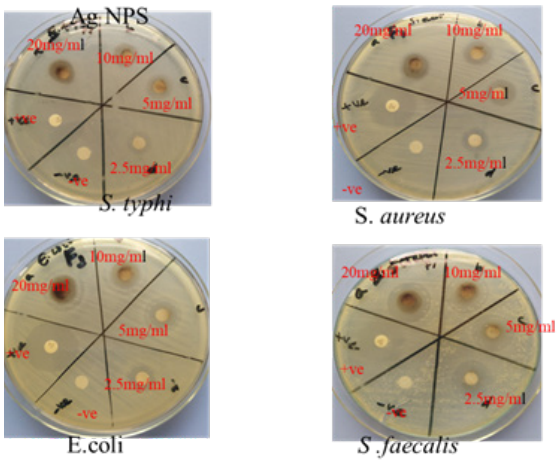

Fig. 10. Antibacterial activities of Ag NPs against *Escherichia-coli*, *Salmonella typhimurium*, *Staphylococcus aureus* and *Enterococcus faecalis*

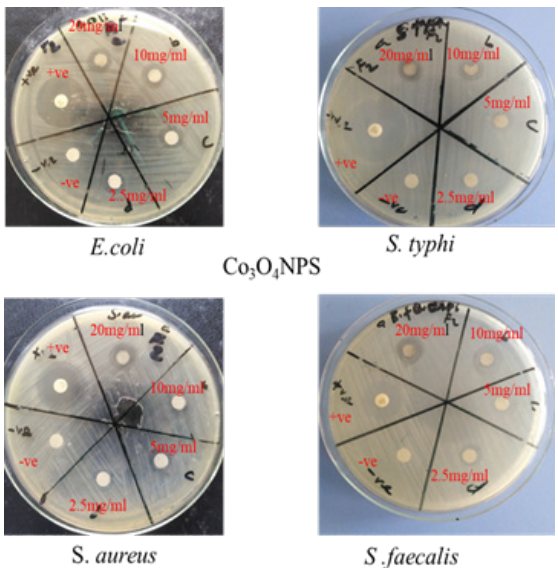

Fig. 11. Antibacterial activities of Co_3O_4NPs against *Escherichia coli, Salmonella typhimurium*, *Staphylococcus aureus* and *Enterococcus faecalis*

The antibacterial activity of the AgNPs and Co_3O_4 NPs was increased with increasing the concentration of the nanoparticles, as demonstrated in (Fig. 10 and 11 supported by Tables 4 and 5). The observed inhibition zone suggests that the disintegration of bacterial species' cell membranes is a necessary step in the biocidal activity of the nanoparticles, which ultimately results in the death of pathogens. As a result, the inhibitory zone size was affected by the pathogen type, the nanoparticle concentration, and the type of nanoparticle. Upon comparing the anti-bacterial activity of green synthesized Ag NPs

Table 4. Zones of inhibition of Ag NPs and Contrimoxazole (+ve control) with different concentrations against different bacterial strains

Sample	Concentration (mg/ml)	Zone of inhibition (mm)			
		Gram-negative species		Gram-positive species	
		Escherichia-coli	*Salmonella typhimurium*	*Staphylococcus aureus*	*Enterococcus faecalis*
Ag NPs	20	16.167 ± 0.167	14.33 ± 0.167	14.167 ± 0.167	21.33 ± 0.33
	10	15 ± 0.2887	13.167 ± 0.167	12.83 ± 0.441	19.3 ± 0.33
	5	12 ± 0.2887	12 ± 0.2887	12.167 ± 0.167	18.33 ± 0.33
	2.5	11.167 ± 0.167	10.33 ± 0.167	10.33 ± 0.167	17.167 ± 0.167
Contrimoxazole (+ve) control		22.83 ± 0.167	23.83 ± 0.167	22	22.167 ± 0.167
DMSO (-ve) control		6	6	6	6

Table 5. Zones of inhibition of Co_3O_4 NPs and Contrimoxazole (+ve control) with different concentrations against different bacterial strains

Sample	Concentration (mg/ml)	Zone of inhibition (mm)			
		Gram-negative species		Gram-positive species	
		Escherichia-coli	*Salmonella typhimurium*	*Staphylococcus aureus*	*Enterococcus faecalis*
Co_3O_4 NPs	20	12.33 ± 0.33	11.83 ± 0.167	10.5 ± 0.2887	12 ± 0.2887
	10	10	9	9 ± 0.5	11 ± 1
	5	9.167 ± 0.167	8.167 ± 0.167	7.667 ± 0.167	8.83 ± 0.167
	2.5	8 ± 0.2887	6	7.167 ± 0.167	7.33 ± 0.167
Contrimoxazole (+ve) control		23	23.833 ± 0.167	22.167 ± 0.167	18
DMSO (-ve) control		6	6	6	6

and Co_3O_4 NPs against the selected bacterial strains (*E. coli*, *S. typhimurium*, *S. aureus*, and *E. faecalis*), Ag NPs showed superior inhibitory activities.

CONCLUSION

The synthesis of Ag NPs and Co_3O_4 NPs using the medicinal plant *C. macrostachyus* has been found to be fruitful. The biogenic synthesized Ag NPs and Co_3O_4 NPs were examined using XRD, UV-DRS, SEM and FTIR. The XRD analysis reveals the formation of crystalline Ag NPs and Co_3O_4NPs with average crystallite sizes of 12.62 nm and 12.746 nm respectively. The energy band gap for Ag NPs and Co_3O_4 NPs was obtained using UV-DRS was found to be 3.38 eV and 3.34 eV, respectively. The phytochemical analysis conducted has confirmed that flavonoids, tannins, terpenoids, glycosides, phytosterols, saponins, and phenols were the major bioactive substances that might be responsible for the reduction of the metal ions during the synthesis of the nanoparticles. The synthesized Ag NPs and Co_3O_4 NPs showed promising antibacterial activity against the studied bacterial strains, *E. coli, S. typhimurium, S. aureus and E. faecalis*. The result proved that Ag NPs showed superior antibacterial activities towards all selected bacterial strains. It can be concluded that biosynthesized Ag NPs and Co_3O_4 NPs mediated by *C.macrostachyus* plant leaf exrtract has the potential to inhibit the disease-causing bacterial strains.

ACKNOWLEDGEMENTS

The authors would like to acknowledge Adama Science and Technology University for supporting this research**.**

FUNDING

The project was financed by the Ethiopian Ministry of Education (MoE) and Adama Science and Technology University.

CONFLICT OF INTEREST

The authors declare that they have no any conflict of interest.

REFERENCES

1. World Health Organization (2014, April), Antimicrobial resistance: Global report on surveillance, (No. 256). Dr Johan Struwe.
2. World Health Organization. (2021), 'Global antimicrobial resistance and use surveillance system (GLASS) report.
3. Fernando S, Gunasekara T, Holton J. Antimicrobial nanoparticles: applications and mechanisms of action. SLJID 2018;8(1):2-11.
4. Guo Z, Chen Y, Wang Y, Jiang H, Wang X. Advances and challenges in metallic nanomaterial synthesis and antibacterial applications. J Mater Chem B. 2020;8(22):4764-4777.
5. Wang L, Hu C, Shao L. The antimicrobial activity of nanoparticles: present situation and prospects for the future. Int J Nanomedicine. 2017;12:1227–1249.
6. Anu Mary Ealia S, Saravanakumar, MP. A review on the classification, characterisation, synthesis of nanoparticles and their application. IOP Conference Series: Materials Science and Engineering. 2017;263(3):032019.
7. Alvi GB, Iqbal MS, Ghaith MMS, Haseeb A, Ahmed B, Qadir MI. Biogenic selenium nanoparticles (SeNPs) from citrus fruit have anti-bacterial activities. Sci Rep. 2021;11(1).
8. Akinsiku AA, Dare EO, Ajani OO, Ayo-Ajayi J, Ademosun OT, Ajayi SO. Room temperature phytosynthesis of Ag/Co bimetallic nanoparticles using aqueous leaf extract of Canna indica. IOP Conf Ser Earth Environ Sci. 2018, 173(1):1-13.
9. Mohammadlou M, Maghsoudi H, Jafarizadeh-Malmiri HJ. A review on green silver nanoparticles based on plants: Synthesis, potential applications and eco-friendly approach. Int Food Res J 2016, 23(2): 446-463.
10. Hafeez M, Shaheen R, Akram B, Haq S, Mahsud S, Ali S, Khan RT. Green synthesis of cobalt oxide nanoparticles for potential biological applications. Mater Res Express 2020, 7(2):1-8.
11. Agilandeswari K, Rubankumar A. Synthesis, characterization, optical, and magnetic properties of Co_3O_4 nanoparticles by quick precipitation. Synth React Inorg Met Org Nano-Met Chem. 2016, 46(4):502-506.
12. Pagar T, Ghotekar S, Pagar K, Pansambal S, Oza R. A review on bio-synthesized Co_3O_4 nanoparticles using plant extracts and their diverse applications. J Chem Rev. 2019;1(4):260-270.
13. Waris A, Din M, Ali A, Afridi S, Baset A, Khan AU, Ali, M. Green fabrication of Co and Co_3O_4 nanoparticles and their biomedical applications: A review. Open Life Sci. 2021; 16(1):14-30.
14. Bawazeer S, Rauf A, Shah SUA, Shawky AM, Al-Awthan Y S, Bahattab OS, El-Esawi MA. Green synthesis of silver nanoparticles using Tropaeolum majus: Phytochemical screening and antibacterial studies. Green Process Synth. 2021 10(1):85-94.
15. Saeed SY, Raees L, Mukhtiar A, Khan F, Khan M, Shah SK. Mazhar K. Green synthesis of cobalt oxide nanoparticles using roots extract of Ziziphus Oxyphylla Edegew its characterization and antibacterial activity. Mater Res Express. 2022; 9(10):1-9.
16. Sun J, Wang Y, Zhang Y, Xu C, Chen H. Egg albumin-assisted hydrothermal synthesis of Co_3O_4 quasi-cubes as superior electrode material for supercapacitors with excellent performances. Nanoscale Res Lett 2019;14(1):340.
17. Urnukhsaikhan E, Bold BE, Gunbileg A, Sukhbaatar N, Mishig-Ochir T. Antibacterial activity and characteristics of silver nanoparticles biosynthesized from Carduus crispus. Sci Rep 2021; 11(1):21047.
18. Mehwish HM, Rajoka MSR, Xiong Y, Cai H, Aadil RM, Mahmood Q, Zhu Q. Green synthesis of a silver nanoparticle using Moringa oleifera seed and its applications for antimicrobial and sun-light mediated photocatalytic water detoxification. J Environ Chem Eng. 2021;*9*(4):105290.
19. Letha N, Ganesan K, Nair PSK, Azalewor HG, Gani SB. Evaluation of *in vitro* antioxidant activity and phytochemical screening of Croton macrostachyus Hochst. by using different solvent extracts. Am J PharmTech Res 2016;6(1):73-85.

20. Obey JK, von Wright A, Orjala J, Kauhanen J, Tikkanen-Kaukanen C. Antimicrobial activity of croton macrostachyus stem bark extracts against several human pathogenic bacteria. J Pathog. 2016;2016:1453428.
21. Gebrehiwota H, Zelelewb D, Gebremariamc H. Chemical analysis and medicinal activities of volatile components from the seeds of Croton macrostachyus plant. Int J Sci Basic Appl Res 2018;37(2):316-330.
22. Riaz M, Ismail M, Ahmad B, Zahid N, Jabbour G, Khan MS et al. Characterizations and analysis of the antioxidant, antimicrobial, and dye reduction ability of green synthesized silver nanoparticles. Green Process.Synth. 2020;9(1):693–705.
23. Gizaw A, Marami LM, Teshome I, Sarba EJ, Admasu P, Babele DA, Abdisa K. Phytochemical screening and in vitro antifungal activity of selected medicinal plants against candida albicans and aspergillus niger in west shewa zone, Ethiopia. Adv Pharmacol Pharm Sci. 2022;2022:3299146.
24. Murthy HCA, Desalegn T, Kassa M, Abebe B, Assefa T. Synthesis of green copper nanoparticles using medicinal plant hagenia abyssinica (Brace) JF. Gmel. Leaf Extract: Antimicrobial Properties. J Nanomater. 2020;2020:1-12.
25. Samuel MS, Selvarajan E, Mathimani T, Santhanam N, Phuong TN, Brindhadevi K, Pugazhendhi A. Green synthesis of cobalt-oxide nanoparticle using jumbo Muscadine (Vitis rotundifolia): Characterization and photo-catalytic activity of acid Blue-74. J Photochem Photobiol B. 2020 ;211:112011.
26. Linh DHT, Anh NP, Mi TTA, Tinh NT, Cuong HT, Quynh TL, Van NTT, Minh NV, Tri N. Biosynthesis, characteristics and antibacterial activity of silver nanoparticles using Lemon Citrus latifolia extract. Mater Trans. 2018; 59(9):1501-1505.
27. Ovais M, Khalil AT, Islam NU, Ahmad I, Ayaz M, Saravanan M, *et al*. Role of plant phytochemicals and microbial enzymes in biosynthesis of metallic nanoparticles. Appl Microbiol Biotechnol. 2018;102(16):6799-6814.
28. Zhou Y, Lin W, Huang J, Wang W, Gao Y, Lin L, et al. Biosynthesis of gold nanoparticles by foliar broths: roles of biocompounds and other attributes of the extracts. Nanoscale Res Lett. 2010;5(8):1351-1359.
29. Ahmad N, Sharma S, Alam MK, Singh V, Shamsi S, Mehta B, Fatma A. Rapid synthesis of silver nanoparticles using dried medicinal plant of basil. Colloids Surf B Biointerfaces 2010;81(1):81-86.
30. Ghoreishi SM, Behpour M, Khayatkashani M. Green synthesis of silver and gold nanoparticles using Rosa damascena and its primary application in electrochemistry. Phys. E: Low-Dimensional Systems and Nanostructures. 2011;44(1):97-104.
31. Raja S, Ramesh V, Thivaharan V. Green biosynthesis of silver nanoparticles using Calliandra haematocephala leaf extract, their antibacterial activity and hydrogen peroxide sensing capability. Arabian J Chem. 2017; 10(2):253-261.
32. Mashwani ZUR, Khan MA, Khan T, Nadhman A. Applications of plant terpenoids in the synthesis of colloidal silver nanoparticles. Adv Colloid Interface Sci. 2016;234:132-141.
33. Vorokh A. Scherrer formula: Estimation of error in determining small nanoparticle size. Nanosyst: Phys Chem Math. 2018;9(3):364–369.
34. Das AJ, Kumar R, Goutam SP. Sunlight irradiation induced synthesis of silver nanoparticles using glycolipid bio-surfactant and exploring the antibacterial activity. J Bioeng Biomed Sci. 2016;6(5):208.
35. Abebe B, Murthy HCA, Zereffa EA, Adimasu Y. Synthesis and characterization of ZnO/PVA nanocomposites for antibacterial and electrochemical applications. Inorg Nano-Met Chem. 2021;51(8):1127-1138.
36. Shrestha S, Adhikari S. Size dependent optical properties of silver nanoparticles synthesized from fruit extract of malus pumila. J Nepal Chem Soc. 2017;37.
37. Vennela AB. Structural and optical properties of Co_3O_4 nanoparticles prepared by sol-gel technique for photocatalytic application. Int J Electrochem Sci. 2019;14(4): 3535-3552.
38. Eltarahony M, Zaki S, ElKady M, Abd-El-Haleem D. Biosynthesis, characterization of some combined nanoparticles, and its biocide potency against a broad spectrum of pathogens. J Nanomater. 2018; (7):1-16.
39. Agilandeswari K, Rubankumar A. Synthesis, characterization, optical, and magnetic properties of Co_3O_4 nanoparticles by quick precipitation. Synthesis and Reactivity in Inorganic, Metal-Organic, and Nano-Metal Chemistry. 2015;46(4):502-506.
40. Farsi M, Farokhi S. Biosynthesis of antibacterial silver nanoparticles by endophytic Fungus Nemania sp. Isolated From *Taxus baccata* Linn. (Iranian Yew). Zahedan J Res Med Sci. 2018;20(6):e57916.
41. Sharma A, Sagar A, Rana J, Rani R. Green synthesis of silver nanoparticles and its antibacterial activity using fungus Talaromyces purpureogenus isolated from *Taxus baccata* Linn. Micro and Nano Systems Letters. 2022;10(1):1-12.
42. Teshale A, Yonas M. Phytochemical investigation and characterization on the stem bark extract of croton macrostachyus. Chem Process Eng Res. 2020;4(6):113-121
43. Asha G, Rajeshwari V, Stephen G, Gurusamy S, Carolin Jeniba Rachel D. Eco-friendly synthesis and characterization of cobalt oxide nanoparticles by sativum species and its photo-catalytic activity. Materials Today: Proceedings. 2022;48:486-493.
44. Bekele ET, Murthy HCA, Muniswamy D, Lemenh YA, Shume MS, Tadesse Ayanie G, et al. Solanum tuberosum leaf extract templated synthesis of Co_3O_4 nanoparticles for electrochemical sensor and antibacterial applications. Bioinorg Chem Appl. 2022;2022:8440756.
45. Kainat Khan MA, Ali F, Faisal S, Rizwan M, Hussain Z, Zaman N, et al. Exploring the therapeutic potential of *Hibiscus rosa* sinensis synthesized cobalt oxide (Co_3O_4-NPs) and magnesium oxide nanoparticles (MgO-NPs). Saudi J Biol Sci 2021;28(9): 5157-5167.
46. Pradeep M, Kruszka D, Kachlicki P, Mondal D, Franklin G. Uncovering the phytochemical basis and the mechanism of plant extract-mediated eco-friendly synthesis of silver nanoparticles using ultra-performance liquid chromatography coupled with a photodiode array and high-resolution mass spectrometry. ACS Sustainable Chem Eng 2021;10(1):562-571.
47. Parlinska-Wojtan M, Kus-Liskiewicz M, Depciuch J. Sadik O. Green synthesis and antibacterial effects of aqueous colloidal solutions of silver nanoparticles using camomile terpenoids as a combined reducing and capping agent. Bioprocess Biosyst Eng. 2016;39:1213-1223.